DOI: 10.65731/ama/2026-0072

A PORT-HAMILTONIAN FRAMEWORK FOR PASSIVE ANALYSIS AND ENERGY-SAFE CONTROL OF COUPLED MOTOR-ROBOT-ENVIRONMENT SYSTEMS

Boaz WADAWA[*], Joseph Yves EFFA[**], Youssef ERRAMI[*], Abdellatif OBBADI[*]

[*]Laboratory: Electronics, Instrumentation and Energy, Department of Physical, Faculty of Science, University Chouaib Doukkali, Eljadida, Morocco
[**]Department of Physics, University of Ngaoundere, P.O. Box 454, Ngaoundere, Cameroon

booz_wadawa@yahoo.fr, effa_jo@yahoo.fr, errami.y@ucd.ac.ma, obbadi.a@ucd.ac.ma

received 28 February 2026, revised 07 June 2026, accepted 10 June 2026

Abstract: This paper proposes a unified and rigorously structured energy-based control framework for a coupled motor-robot-environment system grounded in the port-Hamiltonian formalism. The approach aims to simultaneously guarantee stability, robustness, and energetic safety in physical human-robot interaction scenarios, particularly in collaborative and humanoid robotics. Unlike conventional methods primarily focused on kinematic or dynamic performance, the proposed strategy explicitly structures power flows and the global energy balance, while embedding ethical considerations related to human supervision and control. The main contribution introduces a two-layer safety architecture: (i) explicit limitation of the power injected by the electric motor, ensuring bounded torque transmission; and (ii) an Energy Tank dimensioned from the maximum gravitational torque $\tau_{gmax} = mg\ell$, derived from the gradient of the potential energy. This dual constraint enforces a strict bound on the total available mechanical energy, preserving passivity, preventing unsafe energy amplification, and guaranteeing that robotic autonomy remains energetically supervised and physically controllable by humans. By exploiting the symplectic structure of the port-Hamiltonian model, the total energy variation is formally linked to power ports and dissipative effects. Simulation results demonstrate enhanced robustness, intrinsic energetic coherence, and ethically-informed control, representing a significant step toward safe, controllable, energy-responsible, and human-conscious robotic architectures.

Key words: Port-Hamiltonian, energy control, collaborative robots, passivity and safety, robotics ethics

1. INTRODUCTION

The rapid evolution of industrial and humanoid robotic systems has transformed numerous sectors, ranging from automated manufacturing to service robotics and medical applications [1]. In this context, cooperative and interactive robots often operate in the presence of human operators or within complex environments, giving rise to significant challenges related to operational safety, diagnostic systems, and optimal energy management.

Furthermore, the rapid growth of automated systems integrating artificial intelligence (AI), machine learning, and large-scale data processing algorithms has been accompanied by a substantial increase in energy demand. The availability of sufficient and properly managed electrical energy has therefore become a critical prerequisite for maintaining the performance, reliability, and operational continuity of intelligent robotic systems. Consequently, the optimization and supervision of energy flows have emerged as major challenges for the sustainable development of robotic technologies and advanced digital infrastructures [2, 3].

From an ethical and societal perspective, numerous researchers have also emphasized the importance of incorporating explicit supervision, safety, and control mechanisms into AI-based autonomous systems. Prominent scientists, including Geoffrey Hinton and Yoshua Bengio, have highlighted the challenges associated with the increasing decision-making autonomy of intelligent systems and the need to establish robust frameworks that ensure their safety, predictability, and alignment with human objectives [1, 4, 5, 6]. In the field of collaborative robotics, these concerns further strengthen the relevance of approaches based on energy-flow regulation, as they help ensure that the robot's physical actions remain continuously supervised, bounded, and compliant with the safety requirements of human-robot interaction.

Traditionally, robotic safety relies on physical barriers or kinematic speed reductions, often codified by standards such as ISO 10218, which defines safety requirements for industrial robots, and ISO/TS 15066, which extends these prescriptions to collaborative robots (cobots) by limiting maximum energy and force in human-robot interaction [7, 8]. However, despite these normative standards, conventional methods remain insufficient to guarantee intrinsic and dynamic energy safety, particularly when controlling energy flows between actuators (electric motors), the robot mechanics, and the physical environment, whether human or material. Without a robust energy control architecture, a robot may inject uncontrolled energy into a physical system, potentially causing unregulated behavior, dangerous impacts, or exceeding safe thresholds [9]. This issue is particularly critical in direct physical human-robot interaction.

Furthermore, optimizing the energy consumption of robots, particularly those integrating advanced control techniques, artificial intelligence algorithms, and Big Data-based approaches, remains a major challenge in mastering next-generation automated technologies. Indeed, while these methods improve performance, adaptability, and decision-making autonomy, they often induce computational and energetic complexity that must be rigorously regulated to ensure efficiency, sustainability, and industrial viability [10, 5, 6]. To address these challenges, a unified energy-based approach founded on the port-Hamiltonian theory provides a powerful framework for describing the dynamics of robotic systems in terms of energy exchange, storage, and dissipation. This formulation offers a natural basis for analyzing passivity, stability, safety, and energy management in dynamic systems. Port-Hamiltonian systems explicitly model the energetic interconnections among subsystems, thereby facilitating the design of control laws that preserve the fundamental principles of energy conservation and dissipation, which are essential for ensuring safe, predictable, and physically consistent interactions [11].

Recent developments have confirmed the growing interest in this formalism across a wide range of robotic and mechatronic applications. For instance, the work reported in [12] employs the port-Hamiltonian framework to develop a control strategy that combines a fuzzy logic controller (FLC) with a particle swarm optimization (PSO)-based adaptive mechanism, with the objective of improving the dynamic robustness of an unmanned aerial vehicle subjected to icing disturbances and measurement noise. These results demonstrate the ability of the port-Hamiltonian formalism to accommodate advanced control strategies while preserving a physically consistent representation of the system's energy exchanges. Moreover, a recent line of research has explored control methods based on energy tanks, which constitute auxiliary state variables representing the available energy and are used to control and limit the power that the system can inject. This architecture guarantees that energy exchanges remain bounded, thus ensuring system passivity even when non-passive control laws are applied [8, 13].

In parallel, the development of robust control strategies for electric motors actuating robots, such as Permanent Magnet Synchronous Motors (PMSM), is crucial to ensure that the mechanical power delivered to the robot is strictly controlled and adapted to safety requirements. In robotic applications, PMSM control must handle disturbances, parametric variations, and complex dynamic requirements, which have led to advances in robust control, based on Lyapunov theory and advanced observers [14]. Moreover, the literature on energy safety in human–robot interaction has highlighted the importance of integrating both dynamic passivity aspects and power/energy constraints to prevent physical injuries and comply with energy safety criteria [15].

1.1. Scientific Problem and Ethical Issues

Despite recent advances in passivity-based control, safety standards, and robust actuator tuning, most existing approaches address these aspects in a fragmented manner. In particular, passivity-based control methods, safety constraints, and robust motor control strategies are generally developed independently, thereby limiting their ability to ensure coherent energy safety at the scale of a coupled robotic system. Furthermore, current efforts aimed at raising awareness of the risks associated with increasing robot deployment are not always accompanied by integrated methodological and technical solutions capable of effectively enhancing the safety of automated systems [1, 4]. Consequently, there remains a lack of systemic approaches capable of providing comprehensive energy supervision of a coupled robotic system, encompassing the electric motor, the robot's mechanical structure, and its dynamic interactions with the environment. This scientific gap constitutes the central research problem addressed in the present work.

From both ethical and operational perspectives, the deployment of interactive robots in human-centered environments requires that their physical actions remain continuously supervised and constrained. This necessitates the implementation of explicit energy-supervision mechanisms capable of ensuring that the robot's behavior remains within physically safe limits. In the absence of such mechanisms, uncontrolled energy transfers may lead to hazardous interactions or unexpected behaviors, representing a major concern in current discussions on safety, accountability, and trustworthiness in autonomous and collaborative systems [1, 9, 4, 5, 6].

In this context, two complementary levels of energy safety appear essential:

– explicit control of the power injected by the electric motor, thereby limiting the amount of energy instantaneously available for mechanical actuation;
– design and supervision of an Energy Tank, which imposes an upper bound on the total amount of energy that can be transferred during interaction.

The integration of these two levels within unified control architecture not only guarantees the dynamic stability and passivity of the overall system but also satisfies the intrinsic safety requirements associated with human-robot interactions.

1.2. State of the art

In recent literature, several contributions have partially addressed these issues:

– Passivity-based control and port-Hamiltonian framework. The modeling and control of robotic systems within the port-Hamiltonian framework have been studied for manipulators and mobile robots, demonstrating the ability of these models to preserve passivity and structure energy-based control laws [16].
– Passivity and safety in human-robot interaction. Recent works have proposed control architectures that guarantee the passivity of robotic systems interacting with humans by combining safety and passivity constraints through filters or targeted impedance designs [15].
– Energy tanks in robotics. The use of energy tanks to guarantee passivity and limit the energy transmitted by the system is an emerging and promising approach, widely explored in both theoretical and applied literature [13].
– Robust PMSM control. Robust methods, including those based on Lyapunov theory and improved observers, have been proposed to enhance PMSM response in the presence of uncertainties and disturbances, which are essential for reliable robotic actuator control [14].
– Normative standards and collaborative safety. Relevant ISO standards (ISO 10218 / ISO/TS 15066) provide a recognized safety framework for human-robot interaction, but they are not sufficient on their own to guarantee dynamic energy safety in complex scenarios [17].

Despite these contributions, there is currently no framework that integrates in a unified manner energy-based modeling, port-Hamiltonian control, supervision through energy tanks, and normative and ethical safety constraints.

1.3. Objectives and contributions of the manuscript

This manuscript proposes a unified framework based on the port-Hamiltonian formalism, aimed at ensuring coherent, stable,

DOI: 10.65731/ama/2026-0072

and safe modeling, control, and energy supervision of coupled motor-robot-environment systems. Unlike existing approaches that address passivity-based control, safety, and energy regulation as separate problems, the proposed framework seeks to bridge several theoretical and methodological gaps related to the global energy supervision of collaborative and intelligent robotic systems.

The main contributions of this work are summarized as follows:

– Proposal of two-layer energy-safety architecture:

The first layer explicitly limits the power injected by the electric motor in order to guarantee controlled torque transmission. The second layer relies on the analytical sizing of an Energy Tank based on the maximum gravitational torque. This dual-layer structure ensures bounded mechanical energy and safe interactions, even in the presence of uncertainties and external disturbances.

– Integration of a unified energy-based framework with emerging intelligent-control paradigms:

This work highlights the relationship between energy management in robotic systems and data-driven as well as artificial intelligence-based approaches. Although such methods enhance autonomy and decision-making capabilities, they also increase the computational and energetic complexity of robotic platforms. In this context, the proposed port-Hamiltonian framework provides a suitable foundation for ensuring efficiency, robustness, and long-term sustainability in next-generation robotic systems.

– Explicit consideration of safety requirements and ethical concerns:

The proposed framework guarantees that both injected and stored energy remain physically bounded and continuously supervised. As a result, it contributes to improving the transparency, predictability, and accountability of collaborative robotic systems operating in human-centered environments.

– Identification of future research directions:

These include experimental validation of the proposed framework, its extension to multi-degree-of-freedom robotic systems, and the integration of machine-learning techniques under passivity constraints to further enhance its applicability, scalability, and practical deployment.

The remainder of this manuscript is organized as follows. Section 2 presents the proposed methodology, detailing the design of the two-level energy-control architecture that integrates motor power regulation and the Energy Tank mechanism within a port-Hamiltonian framework. Section 3 is devoted to the presentation and discussion of the results, including the validation of the Permanent Magnet Synchronous Motor (PMSM) control laws and the evaluation of the energy dynamics of the coupled motor–robot–environment system. Finally, Section 4 concludes the paper and outlines future research perspectives.

2. METHODOLOGIES

The proposed secure robotic system (Fig. 1) is based on the analysis of the role of the electric motor in the energy transmission dynamics of the robot. Electric machines, particularly Permanent Magnet Synchronous Machines (PMSM), have the primary function of supplying the industrial robot with a mechanical torque τ_m, as illustrated in Fig. 1. This torque τ_m constitutes the passive power port of the system, representing the fundamental energy exchange variable. It can be regulated or optimized through current control using static converters on the grid side (GSC) and on the machine side (RSC). The DC bus ensuring the interconnection of the two converters guarantees voltage level stability and control of the power flows injected into the machine.

The transmission dynamics between the motor shaft and the robotic arm joint involve several essential mechanical parameters: the viscous friction coefficient F_m, the moment of inertia J_m, the mechanical speed ω_m, as well as the different applied torques such as the motor torque τ_m, the energy regulation torque τ_{tank}, and the environment-related resisting torque τ_{env}.

Thus, the complete motor-robot-environment coupling at the joint level, formulated within the Port-Hamiltonian Interconnection and Damping Assignment-Passivity-Based Control (IDA-PBC) control framework, combined with the appropriate selection of the energy tank energy Etank, makes it possible to guarantee:

– stable interaction with the environment;
– compliance with the passivity properties of the system;
– operational safety, and controlled management of the energy consumption of the robotic arm.

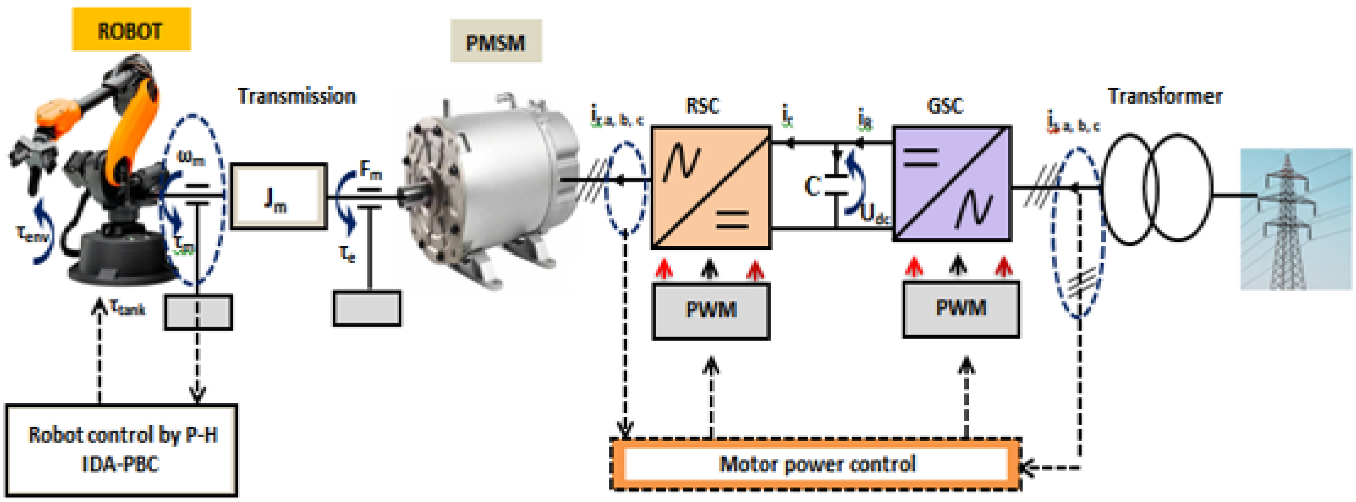

Fig.1. Safe dynamics of the robotic industrial system

2.1. Modeling and control of the PMSM for coupling and secure control of robots

The first level of the safety formalism of the industrial robotic system (Fig.1) concerns the control of the Permanent Magnet Synchronous Motor (PMSM). The objective is to impose strictly controlled energy supply, so that the robot evolves according to its intrinsic dynamics, without excess or energy instability. Regardless of the considered robotic architecture-humanoid or industrial-the control of electric actuators plays a central role in two respects. On the one hand, it enables optimization of the overall energy consumption of the system. On the other hand, it ensures precise control of the injected power, whether remotely or in situ, in order to prevent any undesired dynamic response, particularly during interaction with the environment. Thus, the energy regulation of the PMSM constitutes the first link in the overall safety mechanism, ensuring that mechanical-level power exchanges remain compatible with the passivity and stability requirements of the coupled motor-robot-environment system.

2.1.1. Electrical modeling of the PMSM

The considered robotic system is based on the equivalent electrical model of the PMSM expressed in the rotating Park reference frame *(d, q)*. This representation allows a decoupled description of flux and torque dynamics, thereby facilitating the synthesis of control laws adapted to the selected energy-based and passive framework. The electrical model is then written as follows [18]:

$$\begin{cases} \frac{di_{sd}}{dt} = \frac{1}{L_d}\left(U_{sd} - R_s i_{sd} + \omega_r L_q i_{sq}\right) & (a) \\ \frac{di_{sq}}{dt} = \frac{1}{L_q}\left(U_{sq} - R_s i_{sq} + \omega_r L_d i_{sd} - \omega_r \Psi_f\right) & (b) \\ \frac{d\Omega}{dt} = \frac{1}{F_m}\left(C_e - C_r - F_m \Omega\right) & (c) \end{cases} \tag{1}$$

where the stator voltage components in the *(d,q)* reference frame are denoted by U_{sd} and U_{sq}, respectively; the permanent-magnet flux linkage per pole is denoted by Ψ_f.

The stator winding resistance is denoted by R_s; the direct-axis and quadrature-axis inductances are denoted by L_d and L_q, respectively; the stator currents in the *(d,q)* reference frame are denoted by I_{sd} and I_{sq}, respectively; the rotational speeds of the rotor and the transmission shaft are denoted by ω_r and Ω, respectively; the moment of inertia of the mechanical transmission is denoted by J_m; the viscous friction coefficient of the mechanical transmission is denoted by F_m; and the total resisting torque is denoted by C_r.

The electromagnetic torque of the machine is written as follows [19]:

$$C_{\mathrm{em}} = \frac{3}{2} p\left(\left(L_d - L_q\right) i_{sd} i_{sq} + \psi_f i_{sq}\right) \tag{2}$$

The expression for instantaneous electrical power is written as:

$$P_t = \frac{3}{2}\left(U_{sd} i_{sd} - U_{sq} i_{sq}\right) \tag{3}$$

2.1.2. Synthesis of the PMSM control law

From equation (1), an algebraic rearrangement makes it possible to establish the PMSM current control model, expressed in the form given in equation (4). This formulation highlights the dynamics of the stator currents in the *(d, q)* reference frame and constitutes the basis for the synthesis of the regulation law.

$$\begin{cases} I_{sd} = \frac{1}{R_s + L_d s}\left(U_{sd} + \omega_r L_q I_{sq}\right) \\ I_{sq} = \frac{1}{R_s + L_q s}\left(U_{sq} - \omega_r\left(L_d I_{sd} + \Psi_f\right)\right) \end{cases} \tag{4}$$

A further rewriting of equation (4) then leads to the expression of the reference voltages required for converter control, also reported in equation (5). This expression explicitly incorporates the dynamic coupling terms:

$$\begin{cases} U_{sd}^{*} = U_{sd} + E_d = \left(R_s + L_d s\right) I_{sd} \\ U_{sq}^{*} = U_{sq} - E_q = \left(R_s + L_q s\right) I_{sq} \end{cases} \tag{5}$$

where $E_d=\omega_r L_q I_{sq}$ and $E_q=\omega_r(L_d I_{sd}+\Psi_f)$ represent the cross-coupling compensation components induced by the rotation of the magnetic field. Their consideration ensures effective decoupling of the dynamics along the direct and quadrature axes.

The introduction of a proportional-integral (PI) controller in equation (5) then makes it possible to establish the open-loop transfer functions (OLTF) and closed-loop transfer functions (CLTF) of the current regulation system. From these expressions, the regulation gains $K_{p(Isd,Isq)}$ and $K_{i(Isd,Isq)}$ are derived as follows:

$$\begin{cases} TFOL_{Isd,Isq} = \dfrac{\dfrac{K_p}{s}\left(s + \dfrac{K_i}{K_p}\right)}{L_{d,q}\left(s + \dfrac{R_s}{L_{d,q}}\right)} \\ TFCL_{Isd,Isq} = \dfrac{1}{1 + \dfrac{L_{d,q}\left(s + \dfrac{R_s}{L_{d,q}}\right)}{\dfrac{K_p}{s}\left(s + \dfrac{K_i}{K_p}\right)}} \approx \dfrac{1}{1 + T_r s} \Rightarrow \end{cases}$$

$$\begin{cases} K_{i\,(Isd,Isq)} = \frac{R_s}{T_r} \\ K_{p\,(Isd,Isq)} = \frac{Ld,q}{T_r} \end{cases} \tag{6}$$

Using the parameters in Table A1 in the appendix for the numerical application of the PI gains in equation (6), and for a damping time constant $T_r=1\ ms$, the following values are obtained: $K_{i(Isd)} = K_{i(Isq)}=958$, $K_{p(Isd)}=5.25$, $K_{p(Isq)}=12$. These parameters ensure fast and stable current dynamics, compatible with the energy control and safety requirements of the robotic system.

2.1.3. Simulation assumptions for the robust PMSM control law

The assumptions adopted for the implementation of the control law do not in any way alter the physical structure of the motor. They essentially aim to structure the energy exchanges in order to enhance system robustness and preserve its passivity properties.

The objective is to channel the electromagnetic power exclusively along the quadrature axis *(q)*, while ensuring structural passivity along the direct axis *(d)*. This strategy reduces perturbation effects related to cross-couplings between current components and improves the stability of the overall dynamic behavior. The assumptions considered are as follows:

– Vector orientation of the energy flux along the *(q)* axis:

The vector control principle imposes that the electromagnetic power depends only on the reference current I_{sqref}. This condition corresponds to opening the energy port on the *(q)* axis, characterized by $U_{sqref}=0$. Thus, the quadrature component becomes the

DOI: 10.65731/ama/2026-0072

unique active power transmission channel.

– Cancellation of the reference current on the *(d)* axis:

Imposing $I_{sdref}=0$ guarantees the absence of active energy contribution on the direct axis. This constraint promotes internal dissipation and stabilizes system dynamics by limiting cross-interactions [18].

– Closure of the energy port on the *(d)* axis:

Applying the condition $U_{sd}=0$ ensures the passivity of the subsystem associated with the direct axis. This port closure reinforces the decoupling of the *(d,q)* dynamics, improves robustness with respect to parametric disturbances, and contributes to overall energetic stability.

Under these assumptions, the electromagnetic torque of the PMSM, converted into mechanical power *(P_m)*, can be expressed as follows [18]:

$$C_{\text{em-ref}} = \frac{3}{2} p\psi_f i_{sq-ref} \approx \tau_m \Rightarrow P_m = \tau_m \omega_m \quad (7)$$

The validation of the robust modeling associated with the PMSM control law, corresponding to the first level of secure power control, is presented in the Results and Discussion section. This validation is based on three distinct simulation scenarios, designed to evaluate the relevance and robustness of the previously formulated assumptions. These tests make it possible to analyze the dynamic behavior of the system, the effective channeling of power along the *(q)* axis, as well as the preservation of passivity properties and energetic decoupling.

2.2. Port-Hamiltonian method and analysis of the energetic dynamics of a robotic arm

In analytical mechanics, the dynamic modeling of robotic arms mainly relies on energy-based formulations grounded in the notions of kinetic energy and potential energy. Classical approaches thus lead to the Newton-Euler, Euler-Lagrange, and Hamilton equations, each providing a particular level of description of the system's dynamic behavior. Among these formalisms, the Hamiltonian representation constitutes the theoretical foundation of the port-Hamiltonian (PH) paradigm, which extends the classical formulation by explicitly integrating power exchanges through interconnection ports. This framework offers a unified systemic description of energy flows, particularly suited to the analysis and control of coupled electromechanical systems. In the context of a robotic arm, the port-Hamiltonian approach makes it possible to coherently model the energy interactions between the motor, the mechanical structure of the robot, and the environment (human or material). This unification of power interface ports provides a natural framework to [19]:

– guarantee the passivity properties of the global system;
– ensure interaction safety;
– enhance robustness against disturbances;
– preserve the coherence and traceability of energy exchanges;
– and optimize energy management within the coupled system.

Thus, energy analysis based on the port-Hamiltonian formalism does not merely constitute an alternative modeling approach, but rather a structuring methodological framework enabling the integration of control, safety, and energy efficiency within a unified approach.

2.2.1. Formalism for energy evaluation and control of a single joint robotic arm

Let us consider a robotic arm as shown in Fig. 2 below, rotating about a jointed axis *(0)*, heavy and rigid. Using the energy provided by the actuator-gear pair (PMSM + gearbox), this arm can be described as follows:

– The distance ℓ is the length of the arm between the rotation axis *(0)* and the center of gravity of the arm at *(G)*;
– The moment of inertia I represent the resistance to rotation of the arm with respect to axis *(0)*;
– The angle θ or q represents the position or generalized coordinate formed by the arm with the vertical of the inertial frame;
– The gravitational acceleration at G is given by the constant $g=9.81 m/s^2$;
– The viscous friction coefficient at the joint is denoted D or B.

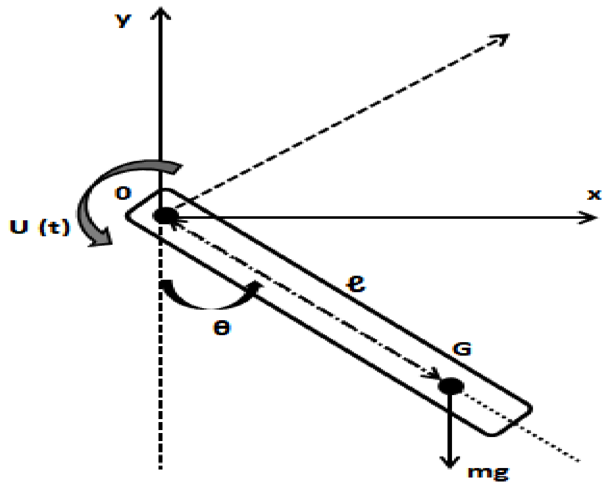

Fig.2. Representation of an articulated robotic arm

2.2.1.1. Determination of the position coordinates and associated energies of the robotic arm

The position coordinates of the arm of length ℓ in the inertial frame are written as:

$$OG(t) = \begin{bmatrix} x_G(t) \\ y_G(t) \end{bmatrix} = \begin{bmatrix} \ell \sin\theta\,(t) \\ -\ell \cos\theta\,(t) \end{bmatrix} \quad (8)$$

The positioning velocity components are written as:

$$v(t) = \frac{d}{dt} OG(t) = \begin{bmatrix} \dot{x}_G(t) \\ \dot{y}_G(t) \end{bmatrix} = \begin{bmatrix} \ell\dot{\theta} \cos\theta \\ \ell\dot{\theta} \sin\theta \end{bmatrix} \quad (9)$$

The expression of the velocity magnitude is written as:

$$v = v(t)^T v(t) = (\ell\dot{\theta})^2 \quad (10)$$

The expressions of the kinetic energy *$T(q,\dot{q})$* and the potential energy *V(q)* of the robotic arm dynamics are written as follows:

$$\begin{cases} T(\theta,\dot{\theta}) = \frac{1}{2} m (\ell\dot{\theta})^2 + \frac{1}{2} I \dot{\theta}^2 \\ V(\theta) = -mg\ell \cos\theta \end{cases} \quad (11)$$

2.2.2. Port-Hamiltonian formalism and energetic dynamics of the robotic arm

The port-Hamiltonian formalism applied to the robotic arm is based on a unified energy framework integrating modeling, control, safety, and observation of power exchanges. This approach is structured around the following principles:

– Hamiltonian energy balance:

The dynamics of the robot and its actuator are described from the Hamiltonian H, representing the total energy of the system (kinetic and potential). Its time evolution H' explicitly reflects the power flows exchanged through the interconnection ports.

– Interconnection and damping assignment-passivity-based control (IDA-PBC):

This strategy makes it possible to act on the interconnection structure and on the dissipation matrices in order to shape a desired Hamiltonian H_d. The latter is designed as a Lyapunov function, guaranteeing asymptotic stability of the closed-loop system while preserving its passivity properties.

– Energetic safety via the Energy Tank (Etank):

The introduction of an energy tank ensures explicit management of energy exchanges by imposing constraints on the available power. This mechanism prevents any energy overflow that could compromise interaction safety.

– Observation of robot-environment interaction:

The analysis of interconnection ports enables a coherent estimation of the energy flows exchanged with the environment, thus providing a direct indicator of the interaction level and safety.

On this basis, the port-Hamiltonian formalism of the robotic arm is developed in five main steps, allowing the structuring of modeling, control synthesis, and the integration of energetic safety mechanisms.

2.2.2.1. Step 1: Determination of the actual energy and the energy balance of the robotic arm

Let us first recall the classical expression of the articulated arm dynamics from the Euler-Lagrange formalism as follows [19]:

$$\frac{d}{dt}\left(\frac{\partial L}{\partial \dot{q}_i}\right)-\frac{\partial L}{\partial q_i}=\tau_i \quad i=1,\dots n \tag{12}$$

Where the set of generalized torque couples associated with the joints and the environment is denoted by τ_i; the generalized coordinates of the joints are denoted by q_i; and the Lagrangian is denoted by $L(q,q')$ and is given by the following expression:

$$\begin{cases}L(q,\dot{q})=T(q,\dot{q})-V(q)\\ L(q,\dot{q})=\frac{1}{2}\left(m\ell^2+I\right)\dot{q}^2+mg\ell cosq\end{cases} \tag{13}$$

The Hamiltonian (H), on the other hand, describes the total energy of the robotic arm through the following function:

$$\begin{cases}H(q,\dot{q})=T(q,\dot{q})+V(q)\\ H(q,\dot{q})=\frac{1}{2}\left(m\ell^2+I\right)\dot{q}^2-mg\ell\cos q\end{cases} \tag{14}$$

The energy balance, as a measurable quantity of the Hamiltonian variable, can be written as:

$$\dot{H}=\frac{d}{dt}H(q,\dot{q})=\frac{H(t+\Delta t)-H(t)}{\Delta t} \tag{15}$$

The port-Hamiltonian equations for conceptualizing the robotic arm are defined as follows [11, 19]:

$$P_i=\left(\frac{\partial L}{\partial \dot{q}_i}\right)\Rightarrow\begin{cases}\dot{q}_i=\frac{\partial H}{\partial P_i}\\ \dot{P}_i=-\frac{\partial H}{\partial q_i}+\tau_i-D\frac{\partial H}{\partial P_i}\end{cases} \tag{16}$$

where D represents dissipation or energy losses.

By rearranging Equation (16), the port-Hamiltonian (P-H) state-space representation of the robot dynamics can be expressed as follows:

$$\begin{bmatrix}\dot{q}_i\\ \dot{P}_i\end{bmatrix}=\begin{bmatrix}0 & I\\ -I & -D\end{bmatrix}\begin{bmatrix}\frac{\partial H}{\partial q_i}\\ \frac{\partial H}{\partial P_i}\end{bmatrix}+\begin{bmatrix}0\\ I\end{bmatrix}\tau_i \tag{17}$$

Furthermore, by identifying the variables and matrices in Equation (17) as: $x'=[q_i'; p_i']^T$, $[J-R]=[0\ I; -I\ -D]^T$, $\nabla H=[\partial H/\partial q_i; \partial H/\partial p_i]^T$, $[G]=[0; I]^T$ and $u=[\tau_i]$, the robot dynamics can be rewritten in the following generalized port-Hamiltonian state-space form [19]:

$$\dot{x}=[J-R]\nabla H+Gu \tag{18}$$

where the matrix (J) represents the interconnection structure matrix, also referred to as the skew-symmetric matrix, which characterizes the internal energy exchanges within the system; the matrix (R) denotes the dissipation matrix, representing the energy losses in the system; the vector (G) corresponds to the port input vector, including the actuators and interactions with the environment; and the variable (u) represents the effort variable applied to the ports, corresponding to the total torques τ_i.

By rearranging equations (16) and (18) in matrix form and exploiting the properties of symplectic geometry, it is possible to express the variation of the system's total energy. This variation, identified as follows, allows direct linking of power flows to port actions and dissipation effects [19]:

$$\dot{H}=\nabla H^T Gu-\nabla H^T R\nabla H\Rightarrow\begin{cases}\nabla H^T Gu\approx\dot{q}\tau_i=\dot{q}(\tau_m^{real}+\tau_{env})\\ \nabla H^T R\nabla H\approx D\dot{q}^2\end{cases} \tag{19}$$

where the term $(\nabla H^T Gu)$ represents the energy injected into and exchanged through the ports; the term $(\nabla H^T R\nabla H)$ represents the dissipated or irreversible internal energy losses; and the variable (τ_i) denotes the port variable, or total effort applied to the mechanical ports, corresponding to the torque generated by the motor and the interaction with the environment.

From equation (19), the expression for the energy balance of the robotic arm can be written as follows:

$$\dot{H}=\begin{cases}P_m+P_{env}-P_d\\ \dot{q}\tau_m^{real}+\dot{q}\tau_{env}-\dot{q}^T D\dot{q}\end{cases} \tag{20}$$

where the mechanical torque, or passive port through which the motor injects mechanical power (P_m) into the arm, is denoted by τ_m^{real}; the term $q'^T Dq'$ represents the dissipation port (P_d), corresponding to the losses due to viscous friction; and the term $q'\tau_{env}$ represents the interaction port power (P_{env}), corresponding to the power exchanged between the robotic arm and its environment.

Within the port-Hamiltonian framework, system passivity is guaranteed when the time derivative of the stored energy remains less than or equal to the power exchanged through the system ports, namely.

$$\dot{H}\le u^T y \tag{21}$$

where y denotes the vector of flow variables associated with (q'). This condition implies that the system cannot generate more energy than it receives from its environment.

The Energy Tank mechanism further strengthens this property

DOI: 10.65731/ama/2026-0072

by imposing an upper bound on the energy available for control actions. As a result, the energy injected into the system remains limited, preventing excessive accumulation of mechanical energy that could compromise either stability or interaction safety. From a Lyapunov perspective, the augmented total energy *(H + Etank)* can be regarded as a positive Lyapunov candidate function whose time evolution remains bounded and dissipative. Consequently, the Energy Tank serves not only as an energy-protection mechanism but also as a means of enhancing system stability by preserving passivity and preventing any uncontrolled amplification of energy exchanges.

2.2.2.2. Step 2: IDA-PBC control law of the Port-Hamiltonian system

Let us rewrite the Hamiltonian *H(p,q)* of the studied robotic arm as follows:

$$\begin{cases} P = \left(\frac{\partial L}{\partial \dot{q}}\right) = \left(m\ell^2 + I\right)\dot{q} \\ H(p,q) = \frac{P^2}{2(m\ell^2+I)} - mg\ell \cos q \end{cases} \tag{22}$$

Let us recall the real port-Hamiltonian formulation in terms of p and q as follows:

$$\begin{cases} \dot{q} = \frac{\partial H}{\partial P} = \frac{P}{m\ell^2+I} \\ \dot{P} = -\frac{\partial H}{\partial q} + \tau_i - D\frac{\partial H}{\partial P} = -mg\ell \sin q + \tau_i - D\dot{q} \end{cases} \tag{23}$$

The objective of the IDA-PBC (Interconnection and Damping Assignment Passivity-Based Control) method is to shape the energy dynamics of the system by imposing a desired port-Hamiltonian structure together with a desired Hamiltonian function (Hd), which are respectively defined as follows [14, 20, 21]:

$$\begin{cases} \dot{q} = \frac{\partial H_d}{\partial P} \\ \dot{P} = -\frac{\partial H_d}{\partial q} - K_d\frac{\partial H_d}{\partial P} \end{cases} \tag{24}$$

where K_d is the derivative damping gain.

$$H_d = \frac{P^2}{2(m\ell^2+I)} + \frac{K_p}{2}(q - q_d)^2 \tag{25}$$

where K_p is the virtual stiffness constant or virtual damping proportional gain, and q_d is the desired generalized coordinate.

It should be emphasized that Equations (24) and (25) are not obtained as a direct mathematical consequence of the preceding equations. Rather, they arise from a design choice inherent to the IDA-PBC methodology, which is based on the principle of energy shaping. More specifically, their formulation is inspired by the structure of the actual port-Hamiltonian system given by Equation (16) and by the expression of the actual Hamiltonian defined in Equation (14). The objective is to define a desired Hamiltonian *(H_d)*, interpreted as a candidate Lyapunov function, in order to shape the dynamics of the robotic manipulator around the desired equilibrium configuration *(q_d)*, corresponding to the strict minimum of the desired energy.

By subsequently substituting the expression of the desired Hamiltonian given in Equation (25) into the desired port-Hamiltonian formulation of Equation (24), the following expression of the desired port-Hamiltonian system is obtained:

$$\begin{cases} \dot{q} = \frac{\partial H_d}{\partial P} = \frac{P}{(m\ell^2+I)} \\ \dot{P} = -\frac{\partial H_d}{\partial q} - K_d\frac{\partial H_d}{\partial P} = -K_p(q - q_d) - K_d\dot{q} \end{cases} \tag{26}$$

The search for the IDA-PBC control law on the port torques τ_i consists of ensuring $H'_d \leq 0$ as a Lyapunov function. To do this, we identify p' in equations (23 and 26) and deduce the expression of the ports associated with the desired energy as follows [14, 20]:

$$\tau_i^{cal} \approx \tau_{IDA-PBC} = mg\ell \sin q - K_p(q - q_d) + (D - K_d)\dot{q} \tag{27}$$

According to the fundamental theorem of rotational dynamics, we can write:

$$\frac{d}{dt}\left(m\ell^2 + I\right)\dot{q} = \tau_i^{cal} \Rightarrow \left(m\ell^2 + I\right)\dot{q} + K_d\dot{q} + K_p(q - q_d) = 0 \tag{28}$$

Equation (28) of the closed-loop dynamics corresponds to the canonical form of the following second-order linear dynamics:

$$\ddot{e} + 2\xi\omega_n\dot{e} + \omega_n^2 e = 0 \tag{29}$$

where the natural undamped frequency is denoted by ω_n; the damping coefficient is denoted by ξ; and the stiffness constant of the energy well is denoted by K_p. By identifying equations (28) and (29), we can write:

$$\begin{cases} \omega_n = \sqrt{\frac{K_p}{m\ell^2+I}} \\ \xi = \frac{K_d}{2\sqrt{K_p(m\ell^2+I)}} \end{cases} \tag{30}$$

The derivations based on Equations (28), (29), and (30) show that the gain K_d is determined from the desired closed-loop dynamics, ensuring a trade-off between response speed and oscillation damping. Consequently, the value of K_d is directly related to the damping ratio ξ, thereby guaranteeing controlled energy dissipation within the system.

In contrast, the Energy Tank parameters are defined from the maximum gravitational torque τ_g^{max}, together with an additional safety margin to ensure passivity and to bound the energy exchanged during operation. These design choices directly affect system stability, torque-limitation capabilities, and robustness against external disturbances.

Compared with conventional control approaches such as PI and LQR controllers, which are primarily focused on reducing tracking errors, the proposed method introduces explicit supervision of energy flows through the combination of the port-Hamiltonian framework and an Energy Tank mechanism. This architecture enables energy constraints to be directly embedded into the control law, thereby simultaneously guaranteeing system stability, passivity, and physical safety.

Recent studies reported in the literature further confirm that energy-based control approaches provide stronger guarantees for robot-environment interactions, particularly in collaborative robotics applications where safety, robustness, and predictable behavior are critical requirements.

The choices of $\omega_n \in$ *[10 to 30] rad/s* and $\xi = 0.023$, corresponding to the desired industrial arm, and using the parameter values from Table A1 in the appendix, allow determining the following K_d and K_p:

$$\begin{cases} K_p = \omega_n^2(m\ell^2 + I) = 10^2(6{,}72) = 672 \\ K_d = 2\xi\sqrt{K_p(m\ell^2 + I)} = 2.0{,}023\sqrt{672.6{,}72} = 3{,}08 \end{cases} \tag{31}$$

The simulation model of the actually desired mechanical torque, associated with the energy tank for safety, obeys the formalism of the IDA-PBC/Energy Tank law as follows [8, 11, 13, 20]:

$$\tau_m^{real} = \begin{cases} \tau_i^{cal}/\tau_{IDA-PBA}, if\ \mathrm{E}_{tank}(\tau_{tank}^{max}) > \mathrm{E}_{min}(\tau_i^{cal}) \\ \tau_{tank}^{max}/\alpha\tau_i^{cal}, \alpha\epsilon]0{,}1[\end{cases} \tag{32}$$

To guarantee passivity and energy safety of the ports, the energy tank *(E_{tank} / τ_{tank}^{max})* serves to limit the injection of motor energy, by considering either the calculated or desired real torque *(τ_i^{cal})* if $E_{tank} > E_{min}$; otherwise, by setting the damping torque *(τ_{tank}^{max} / α τ_i^{cal})*.

The choice of the tank energy *(E_{tank})*, in accordance with ISO-type standards in robotics [8, 21, 22], allows writing:

$$\tau_{Tank}^{max}\epsilon[1{,}5\ 2]\tau_g^{max} \tag{33}$$

where τ_g^{max} represents the maximum gravitational torque.

In practice, the gravitational torque *(τ_g)* corresponds to the gradient of potential energy and takes into account both:

- the local peak or maximum static load at the joint;
- and the minimum energy required to lift the robot's mechanical link.

Meanwhile, the Energy Tank (Etank) acts as an energy-supervision mechanism designed to limit the amount of energy that can be injected into the robot-environment interaction. Its sizing is based on the maximum gravitational torque that may be exerted at the robot joint. This torque is defined as $\tau_g^{max}=mg\ell$ and corresponds to the worst-case static load that the system must be able to compensate.

To introduce a safety margin ensuring both system passivity and the robustness of energy exchanges, the tank-sizing coefficient is selected within the safety interval *(1.5, 2)*, as specified in Equation (33). In the present study, the most conservative choice is adopted by setting this coefficient equal to 2. The maximum admissible torque associated with the Energy Tank is therefore defined as:

$$\tau_{Tank}^{max} = 2\tau_g^{max} \tag{34}$$

The factor 2 is a dimensionless safety coefficient and should not be interpreted as a torque value under any circumstances. Consequently, the quantity τ_{tank}^{max}*(N.m)* represents the only torque bound employed in the proposed energy-supervision mechanism. It defines the upper limit of the energy exchanges authorized by the control law and ensures that the available mechanical energy remains compatible with the passivity, stability, and safety requirements of the robot-environment system.

For the studied robotic arm, whose joints are rigid and subject to gravity, these considerations allow establishing the following relations [8, 21, 22]:

$$\begin{cases} E_{Tank}^{max} \geq \Delta V = V(q_1) - V(q_0) = mg\ell \sin q \\ \tau_g(q) = \frac{\partial V(q)}{\partial q} = mg\ell \sin q \\ \tau_g^{max} = max\left|\frac{\partial V(q)}{\partial q}\right| = mg\ell|\sin q| \end{cases} \tag{35}$$

Using equation (35), it is possible to determine the maximum tank torque (τ_{tank}) not to be exceeded in the studied model. Hence, the maximum gravitational torque τ_g^{max} is reached for $|sinq| = 1$, which leads to: $\tau_g^{max} = m\ g\ \ell = 12 * 9.81 * 0.6 = 70.632$ *N.m*.

From equation (34), the maximum energy tank torque is then calculated as follows: $\tau_{tank} = 2 * \tau_g^{max} = 141.264$ *N.m*.

This value *(τ_{tank})* defines the available power limit in the tank, ensuring that the port-Hamiltonian control remains passive and safe, while covering the maximum energy requirements of the robotic arm during operations under gravitational load.

2.2.2.3. Third step: Validation of safety bounds and local performance of the torque model

The objective of this step is twofold:

- verify energy safety: demonstrating that, regardless of variations in energy exchanges, the torque or effective energy remains bounded by the global safety limit defined by the tank *(τ_{tank}^{max})*;
- evaluate local performance: analysis of the accuracy of the exact torque model around the desired set point, in order to guarantee dynamic behavior consistent with control objectives.

For this, the following parameters are used in equation (27) of the torque:

D - K_d = -3.07 N.m, $mg\ell$ = 70.632 N·m²/s², K_p = 672

This leads to the calculated torque expression: $\tau_{cal} = 70.632 \sin(q) - 672\ (q - q_d) - 94.07\ q'$

The simulation assumptions adopted are as follows:

- Four desired positions q_d, representative of physically significant configurations: *q_d = (0°, 0 rad); (30°, 0.524 rad); (45°, 0.7854 rad); (90°, 1.571 rad);*
- The arm is initially at rest, $q' = 0°$, at critical static instants;
- The maximum tank limit is $\tau_{tank}^{max} = 2 * |\tau_g| = 141.264$ *N.m*.

This configuration allows verification that the calculated torque τ_{cal} remains strictly below the safety limit τ_{tank}^{max} while evaluating the local fidelity of the model with respect to the setpoint q_d.

a) Validation of Etank safety bound

The static equilibrium condition corresponds to:

$\Delta q = q - q_d = 0$ *and* $q = q_d$

The calculated torque values τcal for the chosen setpoint angles are as follows:

τ_{cal} (0) = 0 N.m; τ_{cal} (30°) = 35.316 N.m; τ_{cal} (45°) = 49.944 N.m; τ_{cal} (90°) = 70.632 N.m

It is observed that for any desired angle $q_d\ \epsilon\ [-180°, 180°]$, the calculated torque systematically respects the conditions: $\tau_{cal} < \tau_{tank}$ *and* $\tau_{cal} = \tau_{real}$

Therefore, the energy tank E_{tank} is always respected, and no exceedance of the maximum torque is observed. This constitutes proof of global safety, independent of the exact configuration of the robotic arm, and guarantees local passivity, even for high K_p gains.

b) Validation of local performance of the exact model

The realism allows considering error variation choices such that *Δq is: (±3°, ±0.05 rad); (±6°, ±0.10 rad); (±7°, ±0.122 rad).* Additionally, $q \neq q_d$ *and* $q' = 0$.

In this validation case, we consider the locally critical desired position $q_d = 90°$. *Therefore,* $q = \Delta q + 90°$*, and we can write:* $\tau_{cal} = 70.632 \cos(\Delta q) - 672 * \Delta q$

The values of τ_{cal} *(90°)* corresponding to the following Δq errors are:

– *For Δq (+0.05, -0.05) rad: τ_{cal} = 36.935 N.m, 104.135 N.m;*
– *For Δq (+0.10, -0.10) rad: τ_{cal} = 3.045 N.m, 137.45 N.m;*
– *For Δq (+0.122, -0.122) rad: τ_{cal} = -11.878 N.m, 152.1 N.m.*

Unlike the static equilibrium study, the exact model reaches and exceeds the saturation performance τ_{tank} = *141.264 N.m*, when at the critical desired state $q_d = 90°$ and for $\Delta q = -0.122$ *rad*. Therefore, we see that τ_{cal} = *152.1 N.m* is greater than τ_{tank} = *141.264 N·m*.

Consequently, we can write: $\tau_{real} = \tau_{tank}$ or $\tau_{real} = \alpha\ \tau_{cal}$; to signify that the sizing is consistent with the energy tank conditions of equation (32).

2.3. Modeling of the complete motor-robot-environment dynamics

The modeling of the complete energy dynamics allows coupling and evaluating the motor-robot-environment interaction, such that:
– The motor provides controlled energy to the robot;
– The Tank control law prevents any violent energy injection, bounding the robot's total energy;
– The environment can only consume or return available energy.

This novel complete coupling model at the robotic arm joint unifies the ports of energy torques that interact with the joint efficiency and the motor's controlled mechanical speed.

Consider the Hamiltonian passivity equation at the joint as follows:

$$N = \frac{\omega_m}{\dot{q}} \Rightarrow \tau_m \omega_m = \tau_g \dot{q} \qquad (36)$$

The classical reduction ratio at the joint is N.

The motor-side energy projection and conservation of power at the joint allow determining the efficiency without dissipation losses as follows:

$$\eta = \frac{\tau_{real} + \tau_{env}}{N\tau_m} \qquad (37)$$

where the mechanical torque injected and current-controlled is denoted by τm; the term $(\tau_{real}/N\eta)$ represents the torque used to move the robot; and the term $(\tau_{env}/N\eta)$ represents the torque exchanged with the environment.

The coupled motor-robot-environment dynamics can be compactly expressed as a residual-torque-driven motor equation, ensuring physical causality and energy consistency. The torque dynamics equation can be written as:

$$\omega_m = \frac{1}{j_m s + F_m} \tau_i \qquad (38)$$

where, small*(s)* is the Laplace operator *(s=jw)*.

To determine the complete coupling, equation (37) is introduced into equation (38) of the energy transmission dynamics, yielding the following complete coupling model:

$$\omega_m = \frac{1}{j_m s + F_m} \left[\tau_m - \frac{1}{N\eta} \left(\tau_{IDA-PBA}^{Tank}(q, \dot{q}) + \tau_{env} \right) \right] \qquad (39)$$

The coupled motor-robot-environment dynamics can be compactly expressed as a residual-torque-driven motor equation, ensuring physical causality and energy consistency.

3. RESULTS AND DISCUSSIONS

The evaluation and validation of the proposed secure energy system for motor-robot-environment coupling are structured around two main stages:
– validation of the assumptions of the robust PMSM control law, corresponding to the first level of secure power control;
– simulated evaluation of the energy dynamics, corresponding to the second level of safety, on the complete motor-robot-environment coupling model.

For this analysis, the PMSM and robot parameters presented in Table A1 (Appendix) were used. All simulations were carried out using Matlab/Simulink software, enabling accurate reproduction of the coupled dynamics and verification of the validity of the safety and energy passivity assumptions over the entire system.

In summary, the parameters reported in Table A1 in the Appendix were selected to comply with the physical constraints of the considered robotic system while satisfying the passivity conditions imposed by the port-Hamiltonian framework. More specifically, both the control gains and the Energy Tank parameters were tuned to ensure system stability, limit excessive energy exchanges, and respect the safety bound defined by τ_{tank}^{max}. Their selection results from a trade-off between dynamic performance, robustness, and energy safety across the different operating regimes investigated.

3.1. Validation test of the assumptions of the robust modeling of the PMSM control law

The validation of the motor control law assumptions consists of verifying the following tests by simulation:
– First test:

The quadrature reference current $I_{sq\text{-}ref}$ is a ramp varying from *0 A to 5 A*, respectively from *0 s to 30* s and from *30 s to 60* s. In addition, we take a current $I_{sd\text{-}ref}$ = *5 A* ($I_{sd\text{-}ref} \neq 0$) and $U_{sd} \neq 0$. The simulation results of Fig. 3 are obtained. Under these conditions, it is observed that the current I_{sd} in Fig. 3a generally follows its reference but undergoes disturbances after each transient regime at times *0 s* and *30 s*. Moreover, in Fig. 3b, the current I_{sq} also follows its reference but exhibits a deviation or tracking error with respect to $I_{sq\text{-}ref}$. These observations indicate that opening the ports ($I_{sd\text{-}ref} \neq 0$ *and* $U_{sd} \neq 0$) increases the sensitivity of the control model to disturbances and reference deviations, highlighting the importance of closing the direct port to ensure the robustness and passivity of the control.
– Second test:

The quadrature reference current $I_{sq\text{-}ref}$ is defined as a ramp, identical to that of the first test. The direct-axis reference current is set to $I_{sd\text{-}ref}$ = *0 A* while the voltage $U_{sd} \neq 0$ *V*. The simulation results are presented in Fig. 4.

In this second test, it is observed that the current I_{sd} in Fig. 4a generally follows its reference but undergoes disturbances after each transient regime, at times *0 s and 30 s*. Meanwhile, in Fig. 4b, the current I_{sq} follows its reference with a very small deviation, indicating good tracking despite the presence of disturbances.

These results show that opening the direct port ($U_{sd} \neq 0$ *V*) leads to increased sensitivity of the control model to disturbances and reference deviations, although the errors remain small on the quadrature axis. This analysis confirms that closing the direct port is essential to maximize robustness and passivity of the control, by minimizing the influence of disturbances on the current dynamics.
– Third test:

The quadrature reference current $I_{sq\text{-}ref}$ is this time defined as a decreasing ramp, from *5 A to 1 A*, respectively over the intervals from *0 s to 30 s* and from *30 s to 60 s*. The direct-axis reference current is set to $I_{sd\text{-}ref}$= 0 A and the direct voltage U_{sd}= 0 V. The simulation results are presented in Fig. 5.

The current I_{sd} in Fig. 5a perfectly follows its reference, without disturbance or accuracy error. In addition, in Fig. 5a, the current I_{sq} also follows its reference, without significant deviation and with almost zero fluctuation.

These results demonstrate that complete port closure *($I_{sd\text{-}ref}$ = 0 A and U_{sd} = 0 V)* eliminates the sensitivity of the control model to disturbances and reference deviations. Thus, this test fully validates the port closure assumption, confirming that the PMSM control law is robust to external disturbances and model variations, and guarantees accurate and stable current tracking.

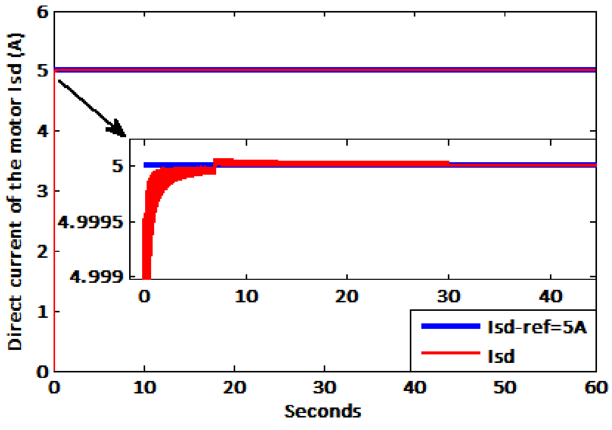

(a)

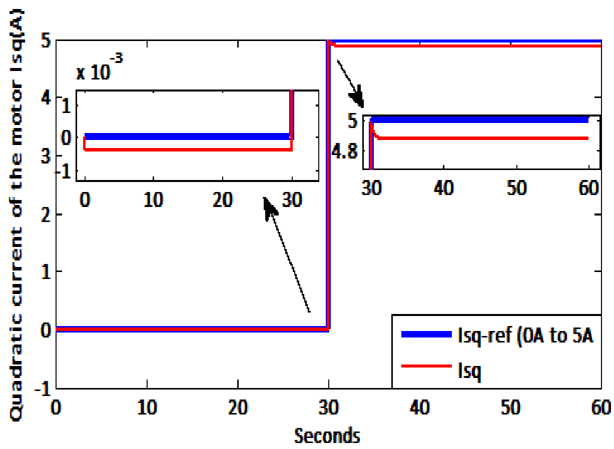

(b)

Fig. 3. Test 1 of current regulation I_{sd}=5A (a) and current control I_{sq}=0A to 5A (b), at U_{sd}≠0

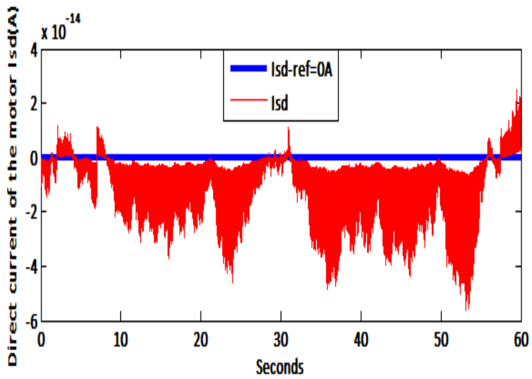

(a)

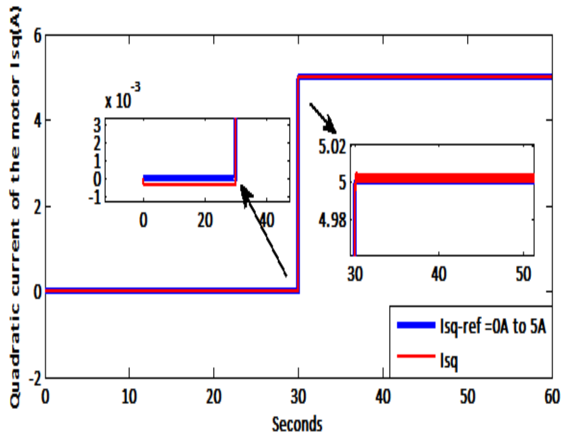

(b)

Fig. 4. Test 2 of current regulation I_{sd}=0A (a) and current control I_{sq}=0A to 5A (b), at U_{sd}≠0V

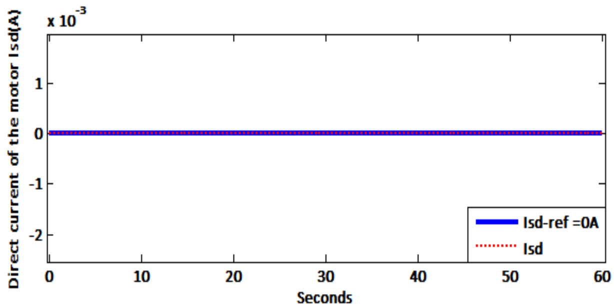

(a)

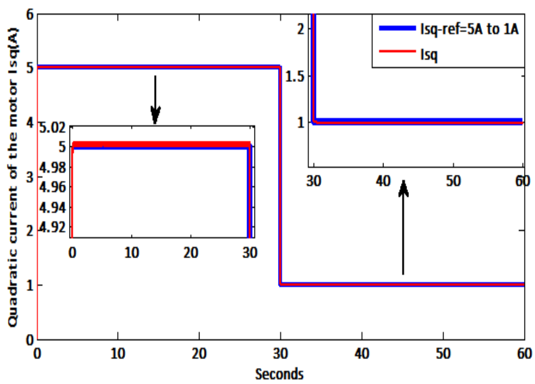

(b)

Fig. 5. Test 3 of current regulation I_{sd}=0A (a) and current control I_{sq}=5A to 1A (b), at U_{sd}=0V

As a preliminary step to the formulation of the hypotheses underlying the robust control law of the Permanent Magnet Synchronous Motor (PMSM) presented in Section 2.1.3, three test configurations were carried out to assess the robustness of different port opening and closing conditions, with the aim of selecting the most appropriate control model for the system.

In summary, the obtained results lead to the following observations:

– First port-opening test *(I_{sd} ≠ 0 and U_{sd} ≠ 0)*:

This case shows that, under the influence of coupling effects represented by the terms *(E_d) and (E_q)* in Equation (5), the control model exhibits sensitivity to disturbances induced by abrupt changes in reference commands *(I_{sdref} = 5 A at t = 0 s, Fig. 3a, and I_{sqref} = 5 A at t = 30 s, Fig. 3b)*. This configuration also leads to a steady-state tracking error between the reference I_{sqref} and the

DOI: 10.65731/ama/2026-0072

actual current *(I_{sq})*, characterized by a relative error of *(E_r = 2.4%)* as shown in Fig. 3b.

– Second partial-port test *($I_{sd} = 0$ and $U_{sd} \neq 0$)*:

In this configuration, the results show that a sudden variation in I_{sq} *(Fig. 4b at t = 30s)* still induces a disturbance on the I_{sd} component *(Fig. 4a at t = 30s)*, indicating that coupling effects *(E_d) and (E_q)* remain present. Moreover, the non-zero voltage port $U_{sd} \neq 0$ introduces additional fluctuations in I_{sd} (Fig. 4a) and contributes to a tracking error between I_{sqref} *and* I_{sq}, with a relative error of *(E_r = 0.1%)* observed in Fig. 4b.

– Third port-closing test *($I_{sd} = 0$ and $U_{sd} = 0$)*:

In contrast to the previous configurations, this case shows that abrupt variations in I_{sq} induce almost no disturbance on I_{sd} *(Fig. 4a, t = 0s and t = 30s)*, indicating a significant attenuation of coupling effects associated with *(E_d) and (E_q)*. Furthermore, simultaneous port closure leads to a reduction in tracking error, with a relative error of approximately *($E_r \approx 0\%$)* observed in Figs. 5a and 5b.

Based on this comparative analysis, the configuration *($I_{sd} = 0$ and $U_{sd} = 0$)* is retained for the subsequent development of the robust PMSM control law. This choice makes it possible to reduce cross-coupling between the *d- and q-axes*, improve the robustness of the motor's dynamic behavior, and ensure better consistency with the passivity and energy-control requirements of the overall motor-robot-environment system.

3.2. Simulated evaluation of the energy dynamics of the second safety level of a complete coupling model (motor, robot and environment)

The simulated evaluation and validation of the secure energy dynamics of the complete coupling system (motor, robot and environment) are carried out through three distinct scenarios:

– No-load or ideal test: the system is tested without compensation of the gravitational torque *(τ_g)*;
– Partial operational test: the system is subjected to partial compensation of the gravitational torque *(τ_g)*;
– Full-load test: the system operates with complete compensation of the gravitational torque *(τ_g)*.

In all simulation cases, the desired robot position is initially fixed at maximum effort, $q_d = pi/2$. The control of the power supplied by the motor is ensured by:

– Regulation of the direct-axis current $I_{sd} = 0$ *A* (fig.5a);
– Control of the quadrature current I_{sq}, set to *5 A* between *0 s* and *30 s*, then to *1 A* between *30 s* and *60 s* (fig.5b).

Figs.5a and 5b illustrate that the power injected by the motor can be controlled precisely and optimally for the robot and, possibly, for its environment. This approach constitutes the first level of energy safety, allowing the human operator to maintain direct control over the energy transmitted to an industrial or humanoid robot.

The second level of energy safety is then evaluated through the three mentioned cases, based on the sizing and simulation of the energy tank Etank, in order to analyze the global energy dynamics of the robot under different load and gravitational compensation conditions.

3.2.1. Case 1 *($I_{sd} = 0$, I_{sq} = 5 A to 1 A, $C_r = 0$, $q_d = 90°$)*: Ideal regime without gravitational compensation

For the no-load regime, the load torque is zero *($C_r = 0$)* and no compensation of the gravitational torque *(τ_g)* is applied. The motor operates in synchronous mode following the I_{sq} reference (fig.5b), thus developing the maximum electromagnetic torque C_{em}, the mechanical speed ω_m, and the instantaneous power P_{int}, as illustrated respectively in Figs.6a and 6b and Fig. 7a.

Fig. 7b shows that the calculated torque τ_{cal} or its estimation correctly follows and bounds the power and respects the Etank limits. Although the upper and lower bounds of the torque τ_{cal} exceed the tank limit (*141.264 N.m)*, the real torque τ_{real} remains limited to the tank value *($\tau_{real} = \tau_{tank}$)*, thus guaranteeing energy safety (fig.8).

Moreover:

– The total energy *H* (fig.9a) reaches its maximum values *(1000 J and 100 J)*, corresponding to the speed ω_m.
– The variation of *H* (fig.9b) stabilizes and oscillates around the maximum values *(500 W and 100 W)* while passing through zero, reflecting instantaneous energy flows.
– Figs.10a and 10b illustrate the maximum environmental power and torque that the robot can withstand within the limits set by *P_{real}, ΔH*, and losses.

In summary, this first scenario demonstrates that:

– All powers are non-zero;
– The motor operates in synchronous mode, providing the maximum possible power;
– The real torque is limited by the tank *($\tau_{real} = \tau_{tank}$)*, ensuring that the robot power threshold is respected;
– The total energy remains below the environmental capacity *(H' < P_{env})*, allowing the robot to withstand or overcome the expected loads without exceeding its limits.

Thus, the ideal case *($C_r = 0$)* is passive, and the motor behaves as an ideal isolating transformer, guaranteeing maximum energy safety while allowing optimal utilization of the available power.

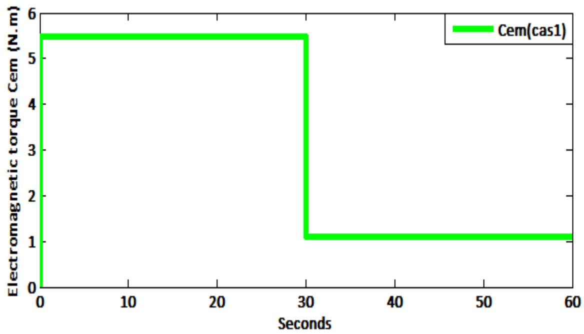

(a)

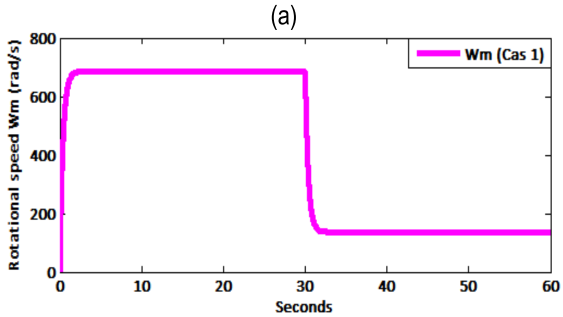

(b)

Fig. 6. Representation of the electromagnetic torque C_{em} (a) and rotational speed W_m (b) of case 1

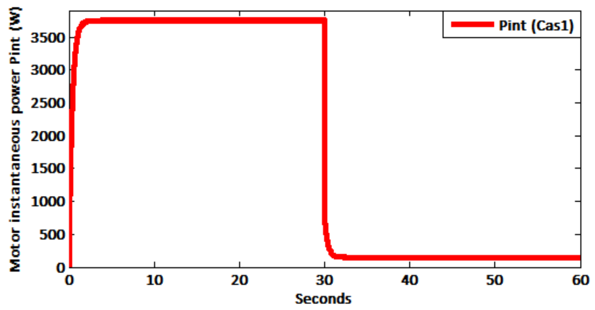

(a)

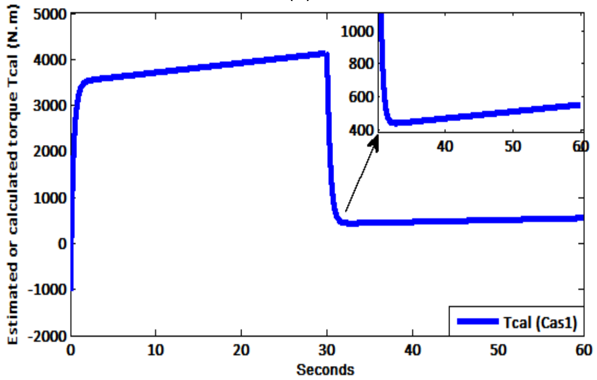

(b)

Fig. 7. Representation of the instantaneous power P_{int} (a) and calculated torque τ_{cal} (b) of case 1

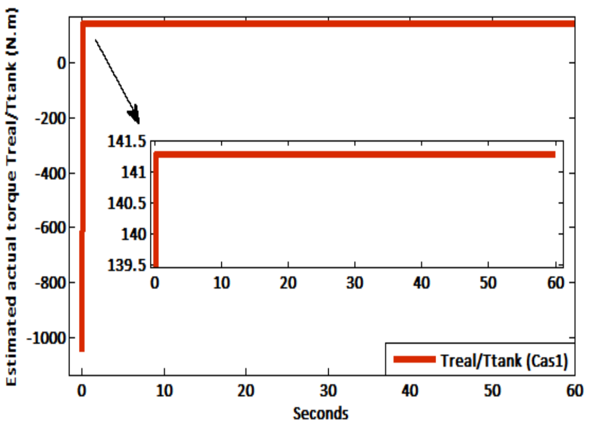

(a)

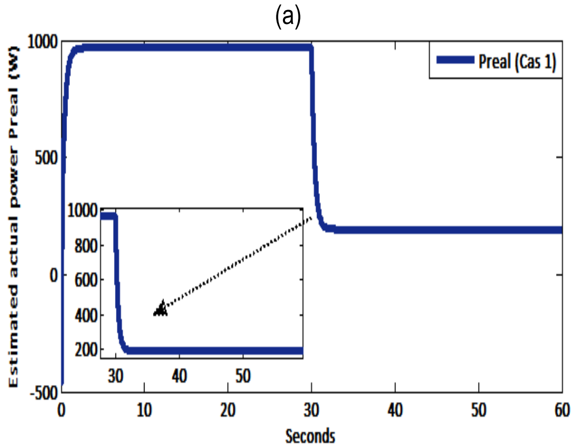

(b)

Fig. 8. Representation of the actual torque τ_{real} (a) and the actual power P_{real} (b) of case 1

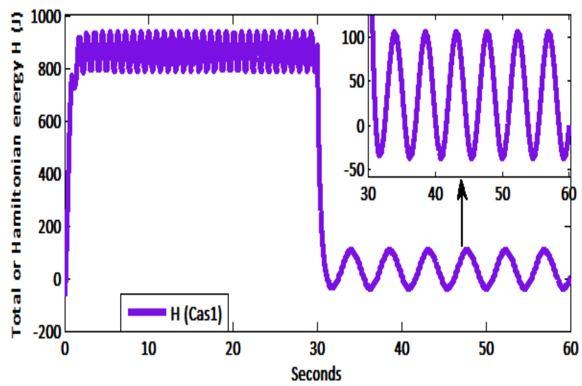

(a)

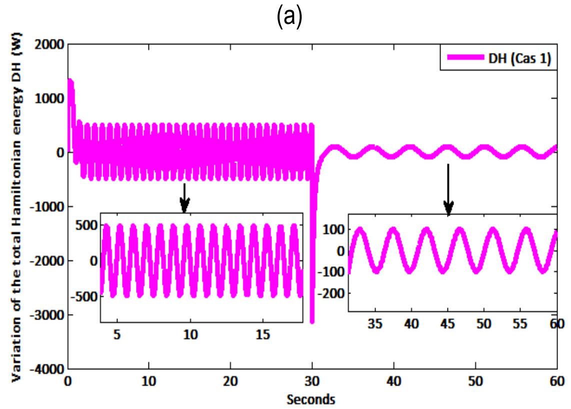

(b)

Fig. 9. Illustration of the total energy H (a) and its change in energy ΔH (b) in case 1

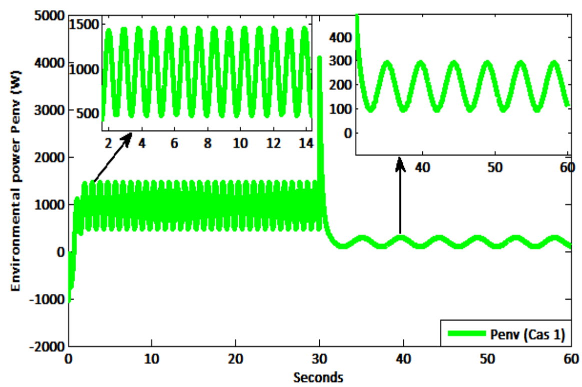

(a)

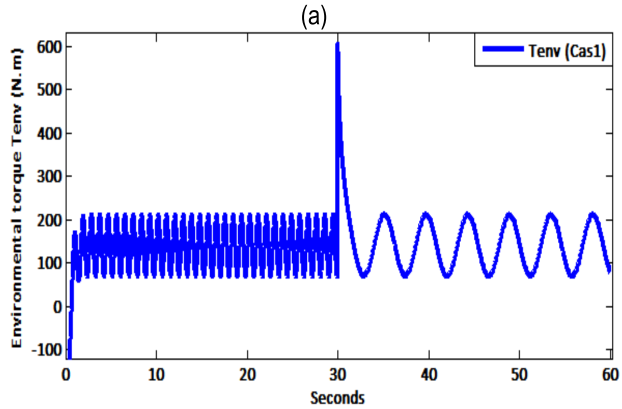

(b)

Fig. 10. Illustration of the environmental power P_{env} (a) and its torque τ_{env} (b) in case 1

DOI: 10.65731/ama/2026-0072

3.2.2. Case 2 ($I_{sd} = 0$, $I_{sq} = 5$ A to 1 A, $C_r = \tau_{real} / N\eta$, $q_d = 90°$): Intermediate regime with partial load compensation

The intermediate regime corresponds to the common operational case, in which the load is partially compensated. Unlike the no-load regime, a decrease in torque, speed, and power is observed, as illustrated respectively in figs.11ab and fig.12a.

Fig. 12b shows that the calculated torque τ_{cal} (or its estimation) correctly follows and bounds the instantaneous power and ensures compliance with the constraint imposed by the E_{tank} reservoir. More precisely, in figs.13ab:

- In the time interval *[0 s, 30 s]*, we have $\tau_{cal} > \tau_{tank}$, which leads to saturation such that $\tau_{real} = \tau_{tank}$;
- In the time interval *[30 s, 60 s]*, we observe $\tau_{cal} < \tau_{tank}$, hence $\tau_{real} = \tau_{cal}$.

Thus, the tank mechanism acts as an adaptive energy bound, limiting the torque when necessary and allowing the system to evolve freely when the energy demand remains below the safety threshold.

Unlike the ideal case, the total energy H (fig.14a) decreases and reaches maximum values on the order of *600 J and 80 J*. Moreover, the time variation of H (fig.14b), as a function of the injected speed ω_m, stabilizes and oscillates around *400 W and 50 W*, periodically crossing zero, which reflects a controlled energy regime.

Figs.15ab also illustrates the power and environmental torque that the robot can withstand, within the limits imposed by P_{real}, ΔH, and internal losses.

In summary, this second scenario highlights that:

- The motor operates with a reduced effort level compared to the ideal case; torques, dissipations, and powers are globally lower;
- The total energy remains below the environmental capacity *($H' < P_{env}$)*, which ensures that the robot can withstand the expected obstacle without exceeding its energy capabilities.

Consequently, this intermediate operational regime satisfies passivity conditions in real operation, confirming the consistency of the tank sizing and the robustness of the energy control in a partially loaded context.

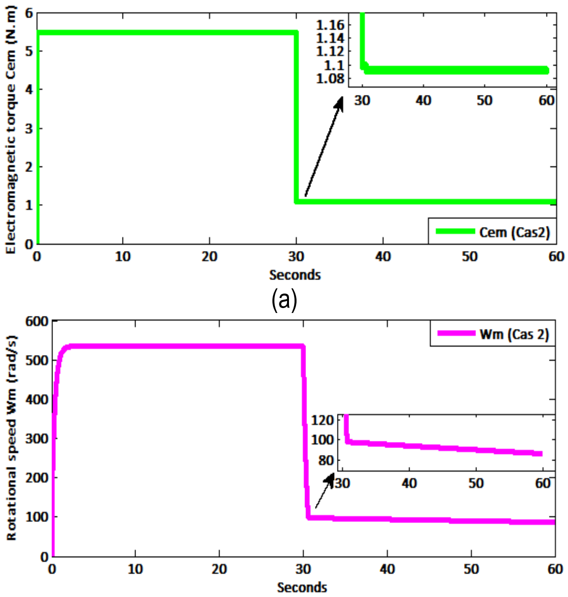

(a)

(b)

Fig. 11. Representation of the electromagnetic torque C_{em} (a) and the rotational speed W_m (b) for case 2

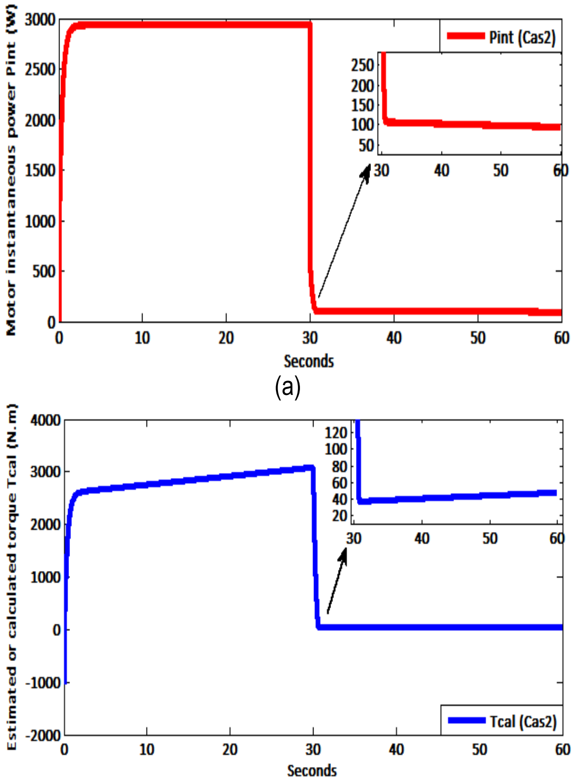

(a)

(b)

Fig. 12. Representation of the instantaneous power P_{int} (a) and the calculated torque τ_{cal} (b) for case 2

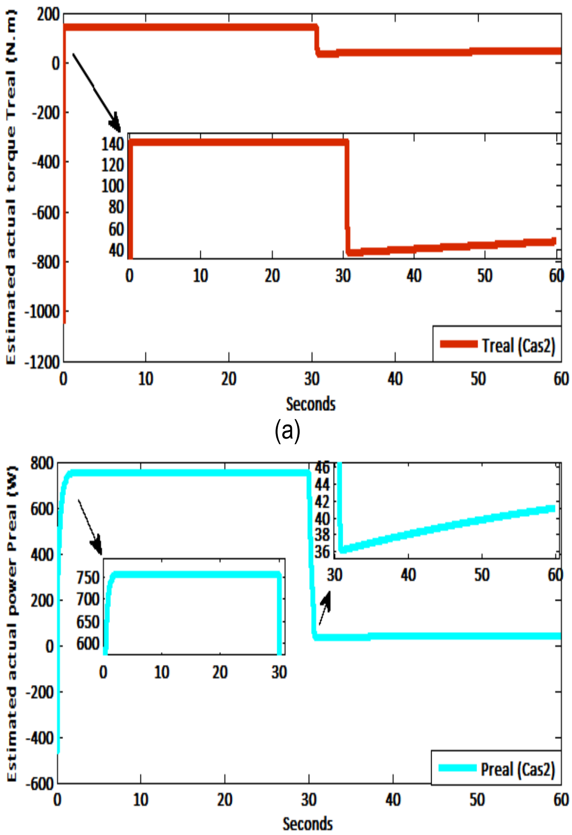

(a)

(b)

Fig. 13. Representation of the real pair τ_{real} (a) and the real power P_{real} (b) of case 2

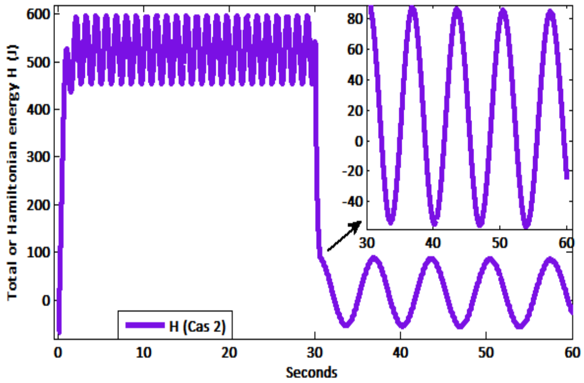

(a)

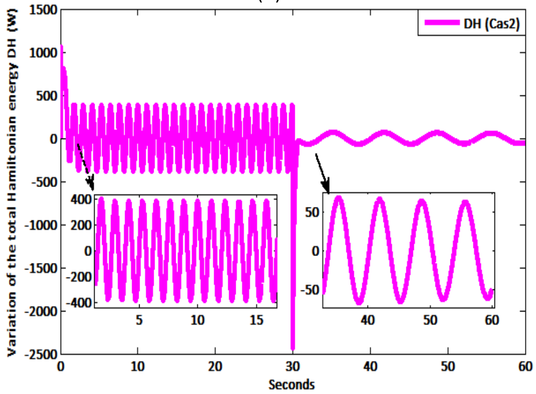

(b)

Fig. 14. Illustration of the total energy H (a) and its change in energy ∆H (b) in case 2

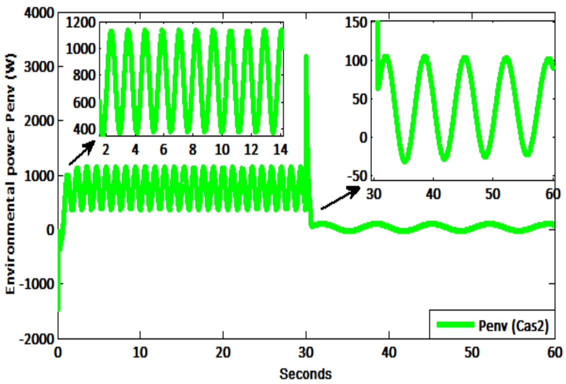

(a)

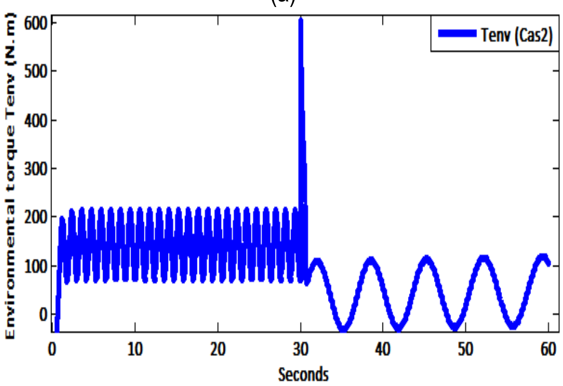

(b)

Fig. 15. Illustration of the environmental power P_{env} (a) and its torque τ_{env} (b) in case 2

3.2.3. Case 3 (I_{sd} = 0, I_{sq} = 5 A to 1 A, $C_r = \tau_g = mgsin(q)$, $q_d = 90°$): Regime with full gravitational compensation

The full-load regime corresponds to the case where the gravitational load is fully compensated. In this configuration, the electromagnetic torque C_{em} (fig.16a) faithfully reproduces the shape of the current I_{sq}, while the rotational speed ω_m (fig.16b) converges toward an equilibrium point close to zero. Consequently, the injected power P_{int} (fig.17a) also tends toward zero.

Fig.17b shows that the calculated torque τ_{cal} (or its estimation) correctly follows the system dynamics and bounds the injected power, while respecting the constraint imposed by the Etank reservoir. Over the time interval *[0 s, 60 s]*, it is observed that $\tau_{cal} < \tau_{tank}$, which directly implies $\tau_{real} = \tau_{cal}$ (fig.17b and fig.18a).

As the speed ω_m becomes nearly constant, the real power P_{real} tends toward zero equilibrium (fig.18b). Unlike the intermediate case, the total energy *H'* (fig.19a) as well as its time variation (fig.19b) progressively vanishes, reflecting an energy equilibrium state. Moreover, the environmental torque τ_{env} converges toward τ_{real} (fig.20b and fig.18b), while the environmental power P_{env} tends toward zero (fig.20a).

This third scenario highlights that:

– The motor operates under nominal load conditions;
– All the power produced by the motor is entirely absorbed by the robot;
– The condition $H' \leq P_{env}$ is satisfied, guaranteeing perfect passivity;
– The rotational speed becomes constant;
– The dynamic quantities no longer drift over time;
– No net power exchange is observed;
– A stable energy equilibrium point is reached.

Thus, the motor operates in a quasi-stationary regime, which can be assimilated to a perfectly coupled ideal transformer, ensuring balanced and fully controlled energy transmission.

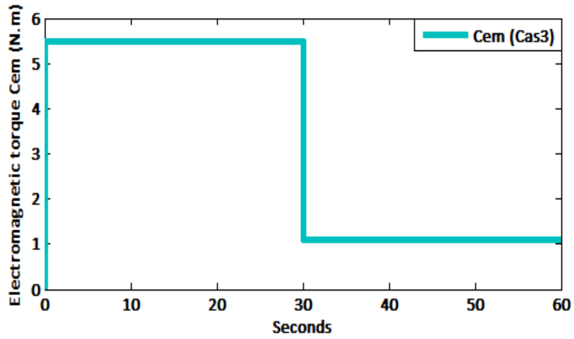

(a)

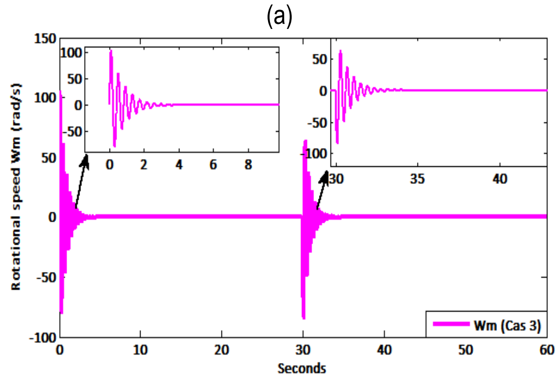

(b)

Fig. 16. Representation of the electromagnetic torque C_{em} (a) and the rotational speed W_m (b) for case 3

DOI: 10.65731/ama/2026-0072

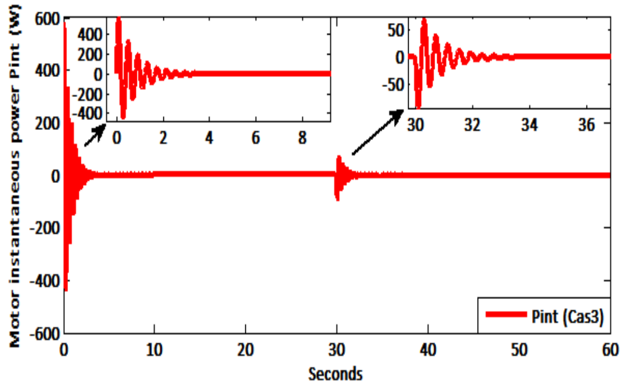

(a)

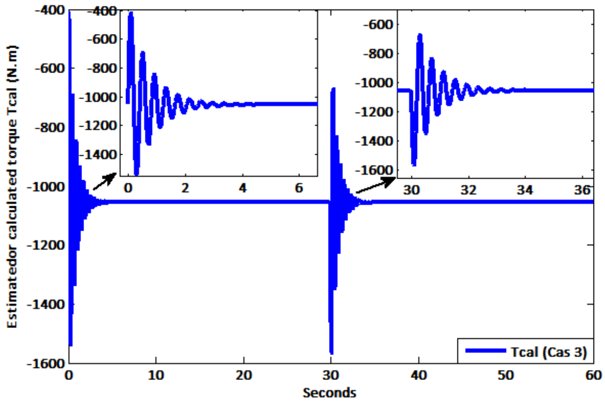

(b)

Fig. 17. Representation of the instantaneous power P_{int} (a) and the calculated torque τ_{cal} (b) for case 3

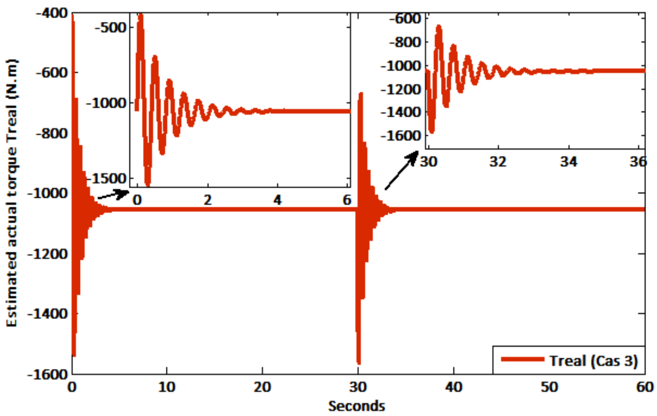

(a)

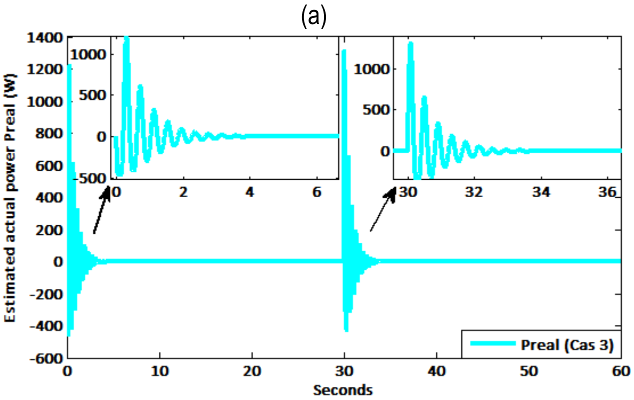

(b)

Fig. 18. Representation of the real torque τ_{real} (a) and the real power P_{real} (b) for case 3

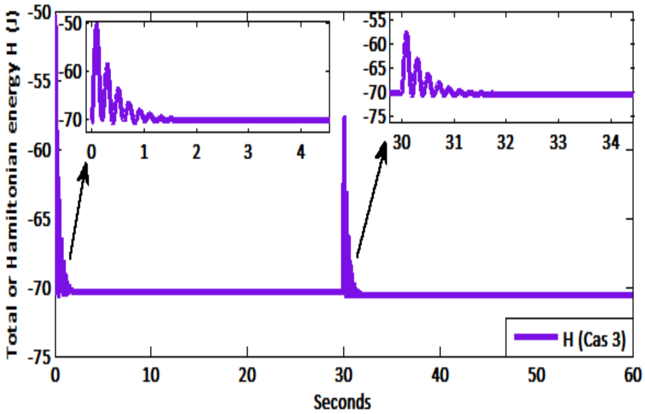

(a)

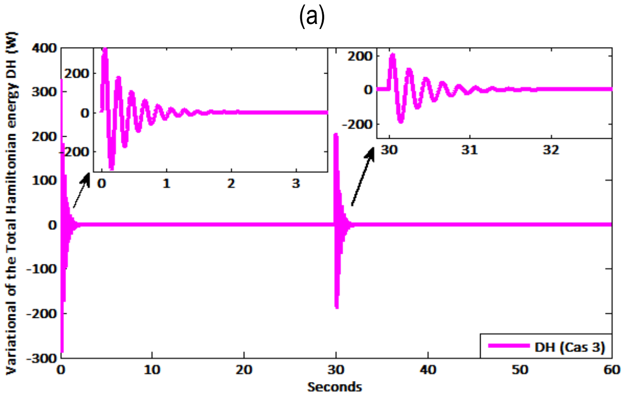

(b)

Fig. 19. Illustration of the total energy H (a) and its change in energy ΔH (b) in case 3

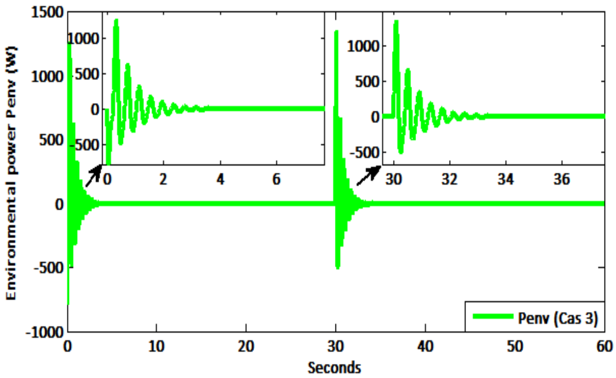

(a)

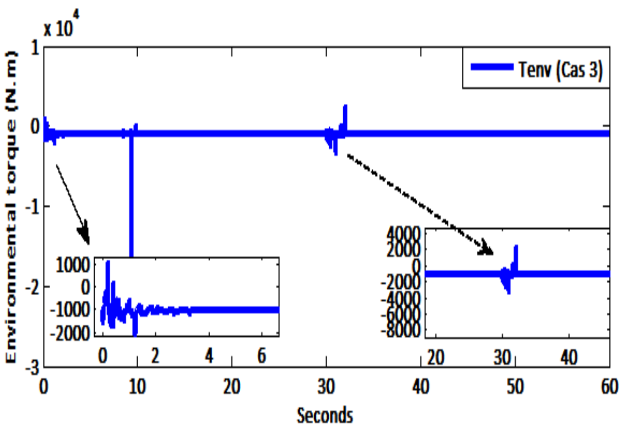

(b)

Fig. 20. Illustration of the environmental power P_{env} (a) and its pair τ_{env} (b) in case 3

In summary, the obtained results call for several additional clarifications to better interpret the highlighted physical phenomena. Within the framework of the studied robotic dynamics, the term ideal transformer refers to a theoretical energy behavior characterized by the absence of internal losses. In this configuration, mechanical power is fully transferred between the motor, the robot, and the environment through the interconnection ports. Conversely, the notion of energy equilibrium corresponds to a steady-state regime in which incoming and outgoing power flows mutually balance each other, resulting in an almost zero variation of the stored energy, *($H' \approx 0$).*

To characterize these phenomena, three operating scenarios were quantitatively compared based on the following indicators:

– The instantaneous power Pint injected by the motor;
– The difference between the computed torque (τ_{cal}), the torque limited by the energy tank (τ_{tank}), and the actually applied torque (τ_{real});
– The variation of the Hamiltonian energy H' with respect to the power exchanged with the environment P_{env}.

The obtained results show that:

a) No-load operation

For the time intervals *[0s, 30s] and [30s, 60s]*, the power injected by the motor is respectively $P_{int} \approx 3{,}7kW$ *and* $P_{int} \approx 151W$ (Fig. 7a). The computed torque reaches $\tau_{cal} \approx 4kN.m$ *and* $\tau_{cal} \approx 450N.m$, respectively (Fig. 7b), while the maximum torque allowed by the energy tank remains fixed at $\tau_{tank} \approx 141{,}5N.m$. It is observed that $\tau_{cal} > \tau_{tank}$. Fig. 8b confirms that the actually applied torque satisfies $\tau_{real} = \tau_{tank}$, reflecting the limiting action of the energy tank. This situation indicates that the available energy is sufficient to drive the system without significant load compensation.

Furthermore, the variations of the Hamiltonian energy are on the order of $H' \approx 1kW$ *and* $200W$ (peak-to-peak values) (Fig. 9b), while the environmental power is estimated at $P_{env} \approx 1{,}1kW$ *and* $210W$ (Fig. 10a). The passivity condition $H' < P_{env}$ is thus satisfied. This no-load regime exhibits the highest energy levels among the three studied scenarios.

b) Partial-load operation

For the same time intervals, the power injected by the motor is respectively $P_{int} \approx 2{,}9kW$ *and* $97{,}1W$ (Fig. 12a). The computed torque reaches $\tau_{cal} \approx 3kN.m$ *and* $\tau_{cal} \approx 45N.m$ (Fig. 12b), while the energy tank limit remains $\tau_{tank} = 141{,}5N.m.$

Over the interval *[0s, 30s],* it is observed that $\tau_{cal} > \tau_{tank}$, leading to $\tau_{real} = \tau_{tank}$. In contrast, over [30s, 60s], the relationship reverses and $\tau_{cal} < \tau_{tank}$, resulting in $\tau_{real} = \tau_{cal}$. This behavior reflects partial load compensation, characteristic of an intermediate operating regime.

Regarding energy exchanges, the variations of the Hamiltonian energy are estimated at $H' \approx 800W$ *and* $110W$ (peak-to-peak) (Fig. 14a), while the environmental power reaches $P_{env} \approx 820W$ *and* $130W$ (Fig. 15a). The passivity condition $H' < P_{env}$ remains satisfied. This intermediate regime is characterized by a trade-off between dynamic performance and energy limitation ensured by the energy tank.

c) Full-load operation

Finally, for the full-load regime studied over the interval *[0s, 60s]*, the injected power tends toward an equilibrium value close to zero *($P_{int} \approx 0$)* (Fig. 17a), while the computed torque reaches $\tau_{cal} \approx 1kN.m$ (Fig. 17b). Since $\tau_{cal} > \tau_{tank}$, the actually applied torque remains limited by the energy tank, $\tau_{real} = \tau_{tank}$ (Fig. 18a).In this case, the variation of the Hamiltonian energy becomes practically zero *($H' \approx 0$)* (Fig. 19a), while the power exchanged with the environment is also $P_{env} \approx 0$ (Fig. 20a). The passivity condition $H' \leq P_{env}$ is therefore satisfied.

Thus, unlike conventional approaches, the proposed control framework ensures an intrinsic limitation of power surges through the energy tank mechanism. This property contributes to improving the robustness of the system against nonlinear interactions and external disturbances, while guaranteeing compliance with passivity and energy stability conditions.

4. CONCLUSIONS

This work establishes a coherent and systemic energy framework for the control of interactive robots, relying on the port-Hamiltonian structure to explicitly link dynamics, power flows, and the overall energy balance. Unlike classical approaches that prioritize tracking performance at the expense of explicit energy analysis, the proposed method enforces intrinsic energy consistency, ensuring stability, robustness, and safety. The central contribution is based on dual-layer energy safety architecture. The first layer involves a direct limitation of motor-injected power, providing strict control of the transmitted torque. The second layer relies on the analytical sizing of the energy tank based on the maximum gravitational torque, ensuring that the total mechanical energy remains bounded by design. This approach eliminates any possibility of uncontrolled energy amplification, even in the presence of parametric uncertainties or external disturbances. Beyond mechanical safety, this contribution addresses a major technological challenge: optimizing the energy consumption of robots integrating advanced control techniques, artificial intelligence, and Big Data-driven approaches. While these technologies significantly enhance performance and autonomous decision-making, they also increase computational complexity and energy consumption. Strict management of energy flows thus becomes essential to guarantee efficiency, sustainability, and industrial viability of next-generation automated systems. From an ethical standpoint, the explicit bounding of injected power and stored energy ensures that robotic autonomy remains energetically supervised and physically controllable by humans. This approach strengthens transparency, predictability, and accountability in collaborative robotic systems. Future directions include experimental validation on real platforms, extension to highly coupled multi-degree-of-freedom systems, and the integration of learning strategies under strict passivity and energy-bounding constraints.

Appendix A

Tab. A1. Simulation parameters for PMSM-Reducer-PI and Robotic Amr-IDA-PBC [12, 16]

<table>
<tr><th>Models</th><th>PMSM+Reducer</th><th>Robotic Arm</th></tr>
<tr><td rowspan="11">Parameters</td><td>U_s = 220V</td><td rowspan="11">m = 12kg
g = 9.81m/s
I=2.4kg.m^2
ℓ=0.6m
D=0.01N.ms/rad</td></tr>
<tr><td>F = 50Hz</td></tr>
<tr><td>R_s = 0.958Ω</td></tr>
<tr><td>L_d = 5.25mH</td></tr>
<tr><td>L_q = 12mH</td></tr>
<tr><td>ψ_f =0.1827wb</td></tr>
<tr><td>p=4 (Pair of poles)</td></tr>
<tr><td>J_m=0.003Kg.m^3</td></tr>
<tr><td>F_m=0.008Nms</td></tr>
<tr><td>N=100(Reduction)</td></tr>
<tr><td>η=0.85 (Efficiency)</td></tr>
<tr><th>Controlers</th><th>PI</th><th>IDA-PBC</th></tr>
<tr><td rowspan="2"></td><td>$K_{p(Isd)}$ = 5.25</td><td>K_p = 672</td></tr>
<tr><td>$K_{i(Isd,\ Isq)}$=958</td><td>K_d= 3.08</td></tr>
</table>

DOI: 10.65731/ama/2026-0072

Parameters	$K_{p(Isq)}$ = 12	τ_{Tank}=145.264N.m
	Tr (ms) = 1	ε=0.023
	ξ =0.7	ω_n=10 rad/s

REFERENCES

1. Wadawa B. Growing Impacts of Robotization and Artifi cial Intelligence for a Global Need to Act Urgently in the Face of the Risks and Potential Damages that Accompany the Development of Human Societies. J Biomed Res Environ Sci. 2023; 4(11): 1582-1585. https://doi.org/10.37871/jbres1833
2. Qing Ch, Yuan T, Li H, Chen Y, Xuehao Wang, Gao S, Ren H, Zhao X, Wang L. A Data-Driven Method for Predicting and Optimizing Industrial Robot Energy Consumption Under Unknown Load Conditions. Actuators. 2024; 13(12): 516. https://doi.org/10.3390/act13120516
3. Suarez E, Bockelmann H, Eicker N et al. Energy-aware operation of HPC systems in Germany. Frontiers in High Performance Computing. 2025; 3: 1520207. https://doi.org/10.48550/arXiv.2411.16204
4. Bengio Y, Hinton G, Yao A et al. Managing extreme AI risks amid rapid progress. Science. 2024; 384(6698);842-845. https://doi.org/10.1126/science.adn0117
5. Hendrycks D. Natural selection favors Ais over humans. arXiv preprint arXiv :2303.16200. 2023. https://doi.org/10.48550/arXiv.2303.16200
6. Bengio Y, Mindermann S, Privitera D et al. International ai safety report. arXiv preprint arXiv: 2501. 17805. 2025. https://doi.org/10.48550/arXiv.2501.17805
7. Tao M. Techman robot targets smart manufacturing market with TÜV professional training for its employees. Robot. Autom. News; 2020.
8. Benzi F, Ferraguti F, Secchi C. Energy tank-based control framework for satisfying the iso/ts 15066 constraint. IFAC-PapersOnLine. 2023; 56(2);1288-1293. https://doi.org/10.48550/arXiv.2304.14059
9. Kalinowska A, Pilarski PM, Murphey TD. Embodied communication: How robots and people communicate through physical interaction. Annual review of control, robotics, and autonomous systems. 2023; 6(1): 205-232. https://doi.org/10.1146/annurev-control-070122-102501
10. Strubell E, Ganesh A, Mccallum A. Energy and policy considerations for deep learning in NLP. In : Proceedings of the 57th annual meeting of the association for computational linguistics. 2019; 3645-3650. https://doi.org/10.18653/v1/P19-1355
11. Li J, Chen Z, Li J et al. Research on rehabilitation robot control based on port-Hamiltonian systems and fatigue dissipation port compensation. Frontiers in Bioengineering and Biotechnology. 2025;13: 1609548. https://doi.org/10.3389/fbioe.2025.1609548
12. Can E. Energy-aware adaptive altitude control of UAVs via fuzzy–PSO optimization within a port-Hamiltonian framework under icing and sensor noise. International Journal of Aeronautical and Space Sciences. 2026; 27(3):2552-2568. https://doi.org/10.1007/s42405-025-01087-2
13. Benzi F, Brunner M, Tognon M et al. Adaptive tank-based control for aerial physical interaction with uncertain dynamic environments using energy-task estimation. IEEE Robotics and Automation Letters. 2022; 7(4):9129-9136. https://doi.org/10.1109/LRA.2022.3190074
14. Zhen S, LI Y, Liu X et al. A Lyapunov-based robust control for permanent magnet synchronous motor in the modular joint of collaborative robot. Robotica. 2023; 41(5): 1389-1406. https://doi.org/10.1017/S0263574722001771
15. Ding Z, Baghbahari M, Behal A. A passivity-based framework for safe physical human–robot interaction. Robotics. 2023; 12(4): 116. https://doi.org/10.3390/robotics12040116
16. Rashad R, Bicego D, Zult J et al. Energy aware impedance control of a flying end-effector in the port-Hamiltonian framework. IEEE transactions on robotics. 2022; 38(6): 3936-3955. https://doi.org/10.1109/TRO.2022.3183532
17. Duplák J, Krajňák F, Yeromina M et al. Application of Safety Standards in the Design of Robotic Workplaces. SAR Journal (2619-9955). 2025;8(4).
18. Yuan M, Meng Y, QI X et al. Research on simulation of permanent magnet synchronous motor in full speed range. Plos one. 2025; 20(4): e0320786. https://doi.org/10.1371/journal.pone.0320786
19. Van Der Schaft A. Port-Hamiltonian modeling for control. Annual Review of Control, Robotics, and Autonomous Systems. 2020; 3(1): 393-416. https://doi.org/10.1146/annurev-control-081219-092250
20. Le LT. Passivity based on energy tank for Cartesian impedance control of DLR space robots with floating base and elastic joints. Journal of Computer Science and Cybernetics. 2018; 34(1):49-62. https://doi.org/10.15625/1813-9663/34/1/11027
21. Siciliano B, Sciavicco L, VillanI L et al. Robotics: modelling, planning and control. London: Springer London. 2009. https://doi.org/10.1007/978-1-84628-642-1
22. Zhong-Ping J, Tao B, Weinan G. Learning-based control: A tutorial and some recent results. Foundations and Trends in Systems and Control. 2020; 8(3):176-284. https://doi.org/10.1561/2600000023

Boaz Wadawa: https://orcid.org/0000-0001-8952-879X

Joseph Yves Effa: https://orcid.org/0000-0002-5812-778X

Youssef Errami: https://orcid.org/0000-0001-8254-5810

Abdellatif Obbadi: https://orcid.org/0000-0001-6936-8485